Int J Adv Manuf Technol (2016) 82:2149–2155
DOI 10.1007/s00170-015-7472-9

ORIGINAL ARTICLE

Effect of microstructure softening events on the chip morphology of AISI 1045 steel during high speed machining

C. L. Pu[1] · G. Zhu[1,2] · S. Yang[3] · E. B. Yue[4] · S. V. Subramanian[5]

Received: 23 March 2015 / Accepted: 22 June 2015 / Published online: 17 July 2015

Abstract The main purpose of this paper is to study the change of chip morphology with increasing cutting speed by considering the role of microstructure evolution in chip root. The orthogonal cutting experiments of AISI 1045 steel showed that the chip morphology would be changed from continuous chip to discontinuous serrated chip as the microstructure softening events occurred in the secondary shear zone with the increasing cutting speed. Based on the principle of cutting force balance and the concept of equilibrium shear angle (ϕ_e), the influence of the dynamic behavior of deformation and recrystallization in chip material on chip morphology was analyzed and modeled. Three types of chip morphology would be characterized corresponding to the sliding, only severe deformation and dynamic recrystallization behaviors, respectively, in the secondary shear zone. It was concluded that the physical mechanism of the serrated chip morphology is the variation of ϕ_e controlled by the mechanical properties of workpiece material in the secondary shear zone, which is related to dynamic deformation behavior of material as influenced by microstructural softening events, such as recrystallization or phase transformation.

✉ G. Zhu
zhugh@ahut.edu.cn

[1] School of Materials Science and Engineering, University of Science and Technology Beijing, Beijing 100083, People's Republic of China

[2] School of Metallurgical Engineering, Anhui University of Technology, Maanshan, Anhui 243000, People's Republic of China

[3] School of Mechanical Engineering, Anhui University of Technology, Maanshan, Anhui 243000, People's Republic of China

[4] National Engineering Research Center of Continuous Casting Technology, Central Iron and Steel Research Institute, Beijing 100081, People's Republic of China

[5] Department of Materials Science and Engineering, McMaster University, Hamilton, ON L8S 4M1, Canada

Keyword High speed cutting · Chip morphology · Dynamic recrystallization

1 Introduction

Lots of the experiments have confirmed that, with the increasing of cutting speed, the chip morphology would gradually be changed from continuous chip to discontinuous serrated chip [1, 2], subsequently resulting in tool accelerated wear [3]. These experimental phenomena have been investigated extensively. Oxley proposed that the severe tool wear was caused by the higher temperature due to high cutting speed without explanation of the relationship between serrated chip and accelerated wear [4]. Karpat et al. claimed that the wear land length is the function of the stresses at flank face, and then computed the value of wear land length at different cutting speeds based on the slip line field theory for steady state cutting [5]. Quiza et al. analyzed the empirical functional relationship between cutting parameters and wear land length, the depth of the crater wear, and the maximum depth of crater by the neural network model and statistical regression model [6]. Kagnayadeng et al. discussed the effect of turning parameters on wear behavior in 1045 steel [7]. However, the physical mechanism of the formation of serrated chip and its relationship to tool accelerated wear is yet to be clarified.

Generally, the cutting process would reach a steady state of constant chip thickness corresponding to an equilibrium shear angle (ϕ_e) as shown in Fig. 1, which depends on the cutting parameters and workpiece properties [8]. That means the cutting balance is not only related to the cutting parameters, but also to the workpiece material [9]. During cutting process, when the mechanical properties of workpiece are changed by microstructural events, the "original balance" has to be destroyed to form a new balance, and correspondingly, the ϕ_e would be varied. As the ϕ_e varied, the thickness of the chip would be correspondingly varied resulting in chip morphology change. In the present paper,

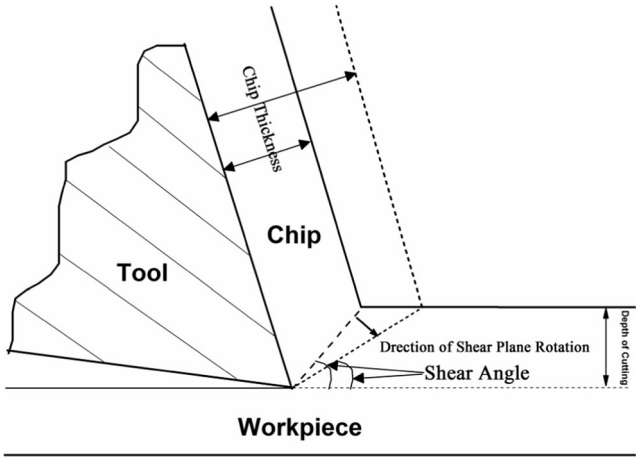

Fig. 1 A schematic diagram showing the rotation of shear angle based on the minimum energy principle

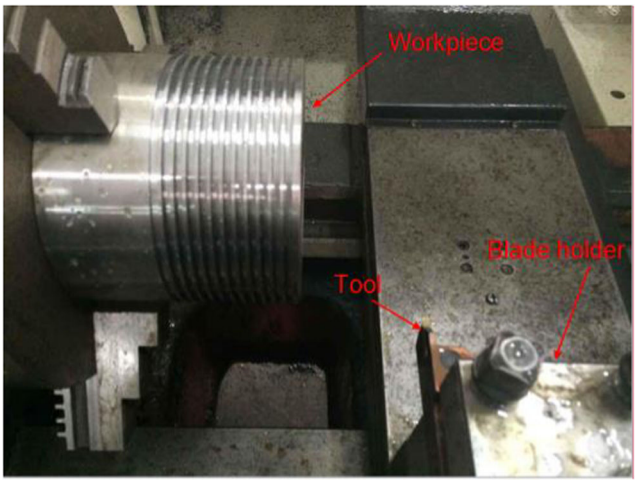

Fig. 2 Experimental setup of orthogonal cutting experiments

the variation of chip morphology due to the dynamic behavior of workpiece materials in the secondary shear zone is analyzed.

2 Experiments

The AISI 1045 steel was used for orthogonal cutting experiments research, and the composition is shown in Table 1. Figure 2 described the experimental setup, where the workpiece of AISI 1045 steel was machined as cylinder with 150-mm diameter and 500-mm length, and a non-coating ISOF (6 % Co) cemented carbide with 0° rake angle and 7° clearance angle was used as cutting tool after mounting on the blade holder. The cutting parameters were feed 0.1 mm, cutting width 2 mm, cutting speed 50~700 m/min. The chips produced in cutting experiment were collected to observe the morphology and microstructure and were examined under by scanning electron microscope (SEM) and optical microscope.

3 Results and discussions

3.1 Characterization of chip morphologies

The typical chip morphologies at different cutting speed are shown in Fig. 3. It can be seen that the macro chip morphologies and microstructures in the secondary shear zone are significantly different at the different cutting speeds. Based on the experimental observation, it was concluded that the chip morphologies could be classified as the following three types: (1) continuous strip chip morphology with small severe strain layer as shown in Figs. 3a, d; (2) continuous strip chip morphology with severe strain layer as shown in Figs. 3b, e; and (3) discontinuous serrated chip morphology with white bright layer as shown in Figs. 3c, f.

Table 1 Chemical composition of the examined steel AISI 1045 (wt%)

C	Si	Mn	P	S	Cr	Ni	Mo
0.43	0.26	0.68	0.01	0.03	0.15	0.1	0.02

The original shear angle was relatively large, close to 45° depending on the rake angle at the beginning of the tool entering workpiece. During the cutting process, the shear angle would be decreased until reached to an "equilibrium shear angle" [10], as shown in Fig. 1. The ϕ_e should be dependent both on cutting parameters and properties of workpiece. Therefore, if the properties of workpiece were changed due to dynamic behaviors of the material, the ϕ_e would be varied corresponding to properties of workpiece to reach "minimum energy" criterion [11].

Generally, the discussion of the deformation behaviors could be divided into two shear zones, i.e., primary shear zone and secondary shear one. The deformation in the primary shear zone could be simplified as shear along the center line of primary shear zone. However, in the secondary shear zone, the chip moves along the tool rake face during which further deformation would occur. At the different shear angle, the shear stress at the interface between tool and workpiece (τ_{int}) would be different from the flow stress of the materials (k_{chip}) which could be calculated by Oxley's model [4]. Depending on the difference between τ_{int} and k_{chip}, the deformation behaviors in the secondary shear zone could be different such as friction, plastic deformation, and microstructure change due to sever heat-force combination, which would play an important role to influence the cutting balance and chip morphology. These are examined in further detail.

Under the condition of low cutting speed, the ϕ_e was correspondingly low. When the tool cuts into the workpiece, and then the shear angle rotates from original value to ϕ_e, the shear stress in the tool/chip interface was not large enough to overcome the flow stress of the workpiece resulting in the further plastic deformation in the secondary shear zone (Fig. 3d). In this case, the dynamic behavior of the workpiece was

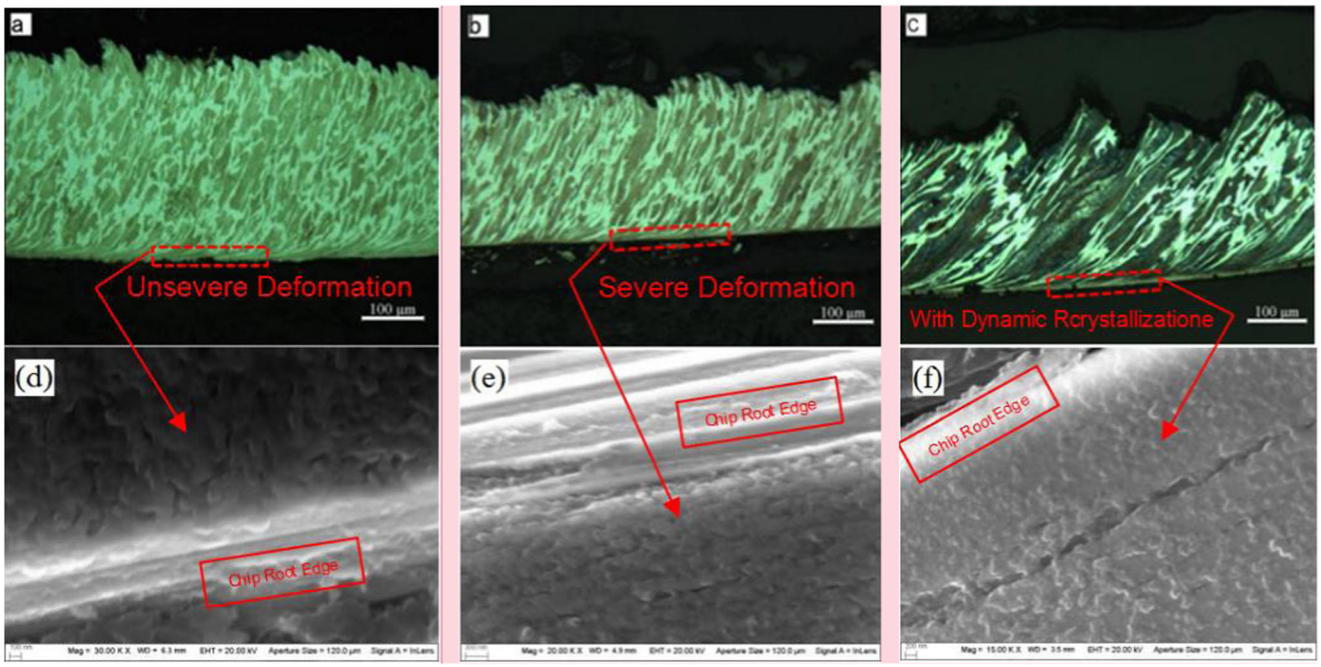

Fig. 3 Typical chip morphology and microstructure in the second shear zone at different cutting speed: 50 m/min (**a**) and (**d**), 150 m/min (**b**) and (**e**), 350 m/min (**c**) and (**f**)

controlled dominantly by the friction between tool and chip, as the chip slides over the rake face. The chip exhibits continuous chip morphology with relatively homogeneous deformation caused in the primary shear zone as shown in Fig. 3a.

With the increase in cutting speed, the shear stress acted in the tool/chip interface was increased due to ϕ_e decreased. It was possible that the applied shear stress in the interface overcame the flow stress of workpiece, the further plastic deformation would be promoted. The deformation would be occurred in a narrow zone of the workpiece in the secondary shear zone to form a severe deformation layer as shown in Fig. 3e, and the chip still exhibits continuous chip morphology (Fig. 3f).

As the cutting speed further increased, the shear stress acted in the tool/chip interface would be further increased resulting in more severe deformation in the workpiece. It should be noted that the deformation heat could not be released in the condition of high speed machining, which would result in local temperature increased. The combination of the temperature and accumulated strain made it possible to promote the dynamic recrystallization or strain-induced phase transformation in the narrow deformation zone resulting in the phenomena of "adiabatic shear band". The dynamic behavior of recrystallization or phase transformation would result in the change of the microstructure in adiabatic shear zone, and subsequently, sharp softening would be occurred in workpiece material at the interface layer. It had to be emphasized that the softening of the workpiece in the secondary zone would result in the increase of ϕ_e. In this condition, it was possible to make the shear angle to be varied between a lower shear angle corresponding to the workpiece with work-hardening state and a larger shear angle corresponding to the workpiece with microstructural softening. The discontinuous serrated chip morphology with "white layer" was observed as shown in Fig. 3c, and the dynamic recrystallization grain can be observed obviously in Fig. 3f. The variation in chip thickness corresponding to variation in equilibrium shear angle caused by periodic microstructural softening event is shown schematically in Fig. 4.

3.2 Modeling the effect of micro-structure on chip morphology

During the cutting process, the deformation of workpiece will occur first in the primary shear zone. And then workpiece "enters" into the secondary shear zone. It should be pointed that the workpiece has been deformed and work hardened in the primary shear zone before entering the secondary shear zone. Therefore, the deformation behavior in the secondary shear zone is deformation of the material that has already undergone deformation in the primary shear zone. The calculation of the strain and material's flow stress due to work hardening in the primary shear zone is the first fundamental step for modeling.

The study of cutting analysis model indicated the state parameters of cutting process for two plastic deformation zones at given shear angle, like geometry size, deformation parameters, and velocity vector diagram. These are illustrated in Fig. 5, where AB corresponded to the primary shear zone and SS represented to the second shear zone.

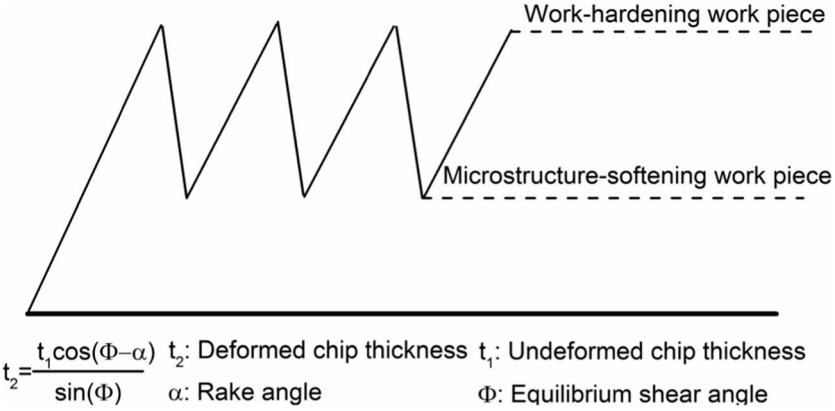

Fig. 4 Sketch of formation of discontinuous serrated chip morphology

Based on Fig. 5, the strain and strain rate in the primary shear zone at given shear angle and other variables could be calculated as follows [4, 5]:

$$\varepsilon_{\mathrm{AB}}=\frac{\cos\alpha}{2\sqrt{3}\sin\phi\cos(\phi-\alpha)} \tag{1}$$

$$\dot{\varepsilon}_{\mathrm{AB}}=\mathrm{C}\frac{V_{\mathrm{s}}}{\sqrt{3}l} \tag{2}$$

$$V_{\mathrm{s}}=V\frac{\cos\alpha}{\cos(\phi-\alpha)} \tag{3}$$

$$l=\frac{t_1}{\sin\phi} \tag{4}$$

$$C=\frac{l}{\Delta S_{\mathrm{p}}} \tag{5}$$

$$\phi_e=\arctan\frac{\frac{t_1}{t_2}\cos(\alpha)}{1-\frac{t_1}{t_2}\sin\alpha} \tag{6}$$

where ϕ is the shear angle, ΔS_{p} is the primary shear zone width, l is the primary shear zone length, C is the strain rate constant for primary shear zone, V_{s} is the shear velocity in primary shear zone, and V is the cutting speed.

In the high speed machining, the heat generated by deformation could not be dissipated and the near adiabatic conditions resulted the temperature rise. The temperature increase due to deformation in the primary shear zone, T_{AB}, could be calculated as [12]:

$$T_{\mathrm{AB}}=T_0+\Delta T \tag{7}$$

$$\Delta T=\frac{(1-\beta)\int_0^{\varepsilon}\sigma(\varepsilon,\dot{\varepsilon},T)d\varepsilon}{C_{\mathrm{p}}\rho} \tag{8}$$

where T_0 is the initial temperature of workpiece (300 K), ρ is the material density of AISI 1045 steel (8000 kg/m^3), $\sigma(\varepsilon,\dot{\varepsilon},T)$ is the flow stress model, β is the percentage of the total plastic deformation energy turning into sensible (90 % in this paper), and C_{p} is the specific heat of AISI 1045 steel as a function of temperature: C_{p}=420+0.504T.

The flow stress of the workpiece is not only the function of strain but also strain-rate and deformation temperature during high speed deformation. Therefore, Johnson-Cook constitutive equation [5, 12–14] was used to calculate the flow stress of the workpiece material in the present work:

$$\sigma=(A+B\varepsilon^{\mathrm{n}})\left(1+CIn\frac{\dot{\varepsilon}}{\dot{\varepsilon}}\left[1-(T^*)^{\mathrm{m}}\right]\right) \tag{9}$$

$$T^*=\frac{T-T_0}{T_{\mathrm{m}}-T_0} \tag{10}$$

The J-C constitutive equation parameters for AISI 1045 steel were summarized in Table 2 [14].

The temperature rise could be calculated as [12]:

$$\int_{T_{\mathrm{W}}}^{T_{\mathrm{AB}}}\frac{\rho(420+0.504T)}{1-\left(\frac{T-T_{\mathrm{W}}}{T_{\mathrm{m}}-T_{\mathrm{W}}}\right)^{\mathrm{m}}}dT=(1-\beta)\left(A\varepsilon_{\mathrm{AB}}+\frac{B}{n+1}\varepsilon_{\mathrm{AB}}^{n+1}\right)\left(1+CIn\frac{\dot{\varepsilon}_{\mathrm{AB}}}{\dot{\varepsilon}_0}\right) \tag{11}$$

Finally, the shear flow stress, k_{AB}, of workpiece after deformation in the primary shear zone could be obtained by the combination of Eqs. (1) to (12):

$$k_{\mathrm{AB}}=\sigma/\sqrt{3} \tag{12}$$

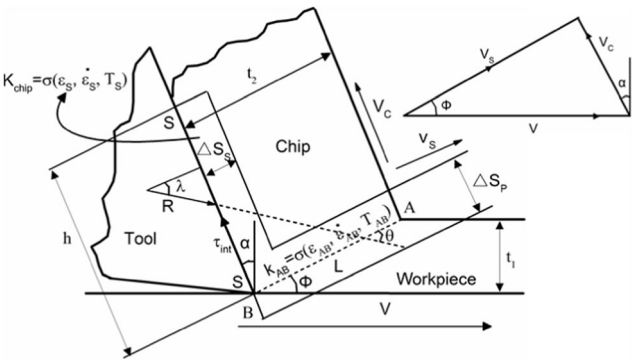

Fig. 5 Schematic diagram of state parameters for two deformation zones at given shear angle

Furthermore, the k_{AB} should be the "initial" flow stress of workpiece when the material enters the secondary shear zone. The applied shear stress, τ_{int}, acted on the tool/chip interface as the function of cutting parameter and material flow stress, could be modeled by Oxley's work based on Eqs. (13)~(16) [4, 8, 9].

$$\theta = \arctan[1 + 2(\pi/4 - \phi) - Cn] \tag{13}$$

$$\lambda = \theta - \phi + \alpha \tag{14}$$

$$h = \frac{t_1 \sin\theta}{\sin\phi \cos\lambda} \tag{15}$$

$$\tau_{int} = \frac{k_{AB} t_1 \sin\lambda}{h \sin\phi \cos\theta} \tag{16}$$

where n is the material constants shown in Table 2, θ is the angle between resultant cutting force (R) and k_{AB}, λ is the friction angle at chip-tool interface, and h is the chip-tool contact length.

The relative relationship between k_{AB} and τ_{int} was calculated as shown in Fig. 6 for low cutting speed (50 and 150 m/min) with the variation of shear angle. As indicated in Fig. 6, the τ_{int} increased with decreasing shear angle, and the effect of shear angle on the k_{AB} was opposite. It could be seen that a shear angle, ϕ_p corresponding to $k_{AB}=\tau_{int}$, is predicted for 50 and 150 m/min to be about 26° and 35°, respectively. Based on the minimum energy criterion, when the total energy in the primary and secondary shear zone reached the minimum, the shear angle would be equilibrium shear angle, ϕ_e, and the cutting process reached stable cutting. Thus, if the equilibrium shear angle ϕ_e is larger than the ϕ_p, the shear angle would be rotated firstly to the ϕ_e and reached stable cutting, resulting in a continuous chip morphology without severe deformation in the secondary shear zone as shown in Figs. 3a, d. However, if the equilibrium shear angle ϕ_e is less than the ϕ_p, the shear angle would be rotated firstly to ϕ_p, and then the applied shear stress τ_{int} would overcome the flow stress of the workpiece k_{AB}, resulting in further plastic deformation in the secondary shear zone. As to this situation, the flow stress in the secondary shear zone could be expressed as:

$$k_{chip} = k_{AB} + \sigma(\varepsilon_s, \dot{\varepsilon}_s, T_s) \tag{17}$$

where ε_s, $\dot{\varepsilon}_s$, and T_s is the strain, strain-rate, and deformation temperature in the secondary shear zone.

$$\varepsilon_s = \frac{h}{2\sqrt{3}\delta t_2} \tag{18}$$

Table 2 J-C follow stress model constants for AISI 1045steel

A (MPa)	B (MPa)	n	C	m	T_m (°C)	T_0 (°C)
553.1	600.8	0.234	0.0134	1	1460	25

$$\dot{\varepsilon}_s = \frac{V_c}{\sqrt{3}\delta t_2} \tag{19}$$

$$\delta = \frac{\Delta S_s}{t_2} \tag{20}$$

$$V_c = V \sin\phi / \cos(\phi - \alpha) \tag{21}$$

where ΔS_s is the thickness of second shear zone, V_c is the chip velocity, and δ is the strain rate constant of second shear zone.

The value of T_s can be calculated by Eqs. (11) and (18)~(21) in the same way as in the computation of T_{AB}.

When the plastic deformation occurred in the secondary shear zone, atomic contact between chip and tool rake face is generally assumed and the sliding friction at chip-tool interface is ignored [15]. In this case, the strain, strain rate, and deformation temperature could be calculated by Oxley's model combining with J-C equation and then the flow stress of the workpiece could be obtained as shown in Fig. 6 at a given cutting speed and feed. Subsequently, work hardening would occur in the secondary shear zone and result in further deformation. The chip morphology was shown in Fig. 3b, and the microstructure in second shear zone was illustrated in Fig. 3e.

The severe deformation in the secondary shear zone should accumulate the strain and increase the temperature. Thus, the microstructural events such as dynamic recrystallization and phase transformation also should be considered. The study of modeling dynamic recrystallization behavior shows the critical strain for dynamic recrystallization (ε_c) could be expressed as [16–18]:

$$\varepsilon_c = A \ln Z^B \tag{22}$$

where A and B are the fitness constant, Z is the Zener-Hollomon parameter, $Z = \dot{\varepsilon}\exp\left(\frac{Q}{RT}\right)$, Q is the deformation energy for deformation, R is the gas constant (8.314 J mol/K).

The research of dynamic recrystallization behavior on AISI1045 steel is published in Ref [19], and the parameters could be deduced by this work, where the value of A, B, and Q is 0.4055, 0.038, and 291 KJ mol^{-1}, respectively.

When the accumulated strain in the secondary shear zone ε_s is large enough to promote dynamic recrystallization ε_c or the deformation heat to increase the temperature higher than the phase transformation temperature, the material of the workpiece would be sharply soften because microstructural events. It would result in the sharp variation of the equilibrium shear angle and lead to the production of discontinuous serrated chip morphology as shown in Fig. 2c. There is metallographic evidence for the occurrence of dynamic recrystallization (Fig. 2f).

It should be pointed that τ_{int} and k_{AB} are the function of cutting speed. Therefore, the ϕ_p and the equilibrium shear angle ϕ_e are also the function of cutting parameters as the results of calculation. As the cutting speed increased, the equilibrium shear angle ϕ_e, the shear angle ϕ_p, where the applied

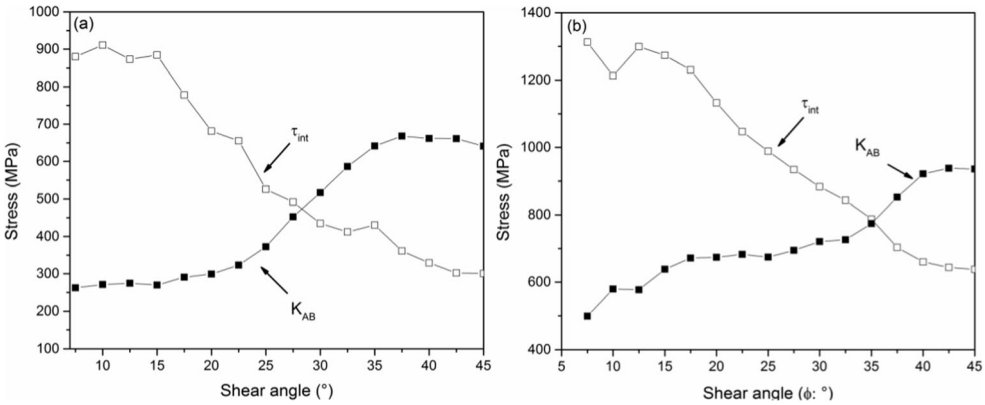

Fig. 6 Plot of of τ_{int} and k_{AB} as a function of shear angle for different cutting speed: **a** 50 m/min, **b** 150 m/min

shear stress is equal to the flow stress of the workpiece, $\tau_{int}=k_{AB}$, and the shear angle where the accumulated strain is equal the critical strain for dynamic recrystallization (or the temperature is equal to the phase transformation temperature), $\varepsilon_s=\varepsilon_c$, were calculated as shown in Fig. 7. It can be seen that the equilibrium shear angle has a maximum value when the cutting speed is less than 75 m/min. In this case, continuous chip morphology would be obtained with an equilibrium shear angle. When the cutting speed increases to larger than 75 m/min but less than 275 m/min, the shear angle would be change from entering angle to ϕ_p and then further plastic deformation would be occurred in the secondary shear zone. In this case, the chip morphology would be continuous with severe deformation in the secondary zone as shown in Fig. 3b. The shear angle would be equilibrium shear angle with work-hardened materials. As the cutting speed increased over 275 m/min, it can be seen that from Fig. 7, the ϕ_R (dynamic recrystallization) would be met before the shear angle reaches the equilibrium shear angle after the severe deformation occurred in the secondary zone. It should be noted that the softening event would be occurred when the dynamic recrystallization was promoted. The shear angle would be inversely rotated to new equilibrium shear angle corresponding to softened workpiece. In this case, the discontinuous serrated chip morphology would be obtained.

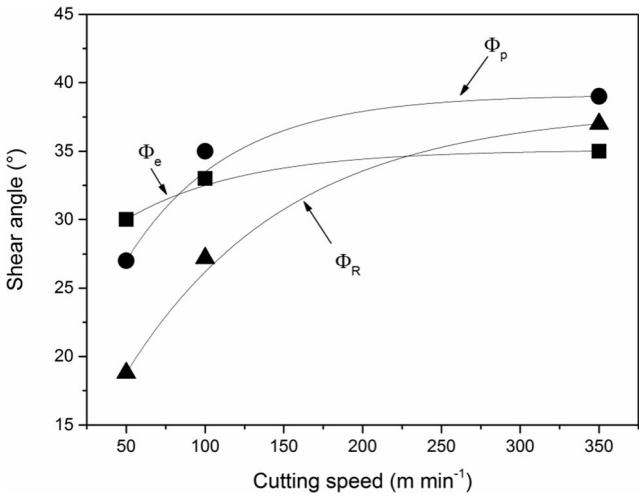

Fig. 7 The effect of cutting speed on ϕ_e, ϕ_p, and ϕ_R

4 Summary

Based on the experimental observation, the physical mechanism of formation of three different chip morphology encountered as a function of cutting speed in AISI 1045 steel is analyzed using Oxley's model for equilibrium shear angle based on the criterion of minimum total energy consumed in the primary and secondary shear zone. At low cutting speed, sliding tribological condition of asperity contact at the tool-chip interface is obtained and there is no severe deformation in the secondary shear zone. The chip morphology is continuous. When the cutting speed is progressively increased, the asperities are squeezed to make atomic contact at the tool-chip interface. There is an onset of severe plastic deformation in the secondary shear zone, when the equilibrium shear angle is decreased with the corresponding increase in chip thickness. Continuous chip morphology will be predicted by Oxley's model even at moderate cutting speeds at the same feed. If the plastic deformation occurred in the secondary shear zone but there is no occurrence of the microstructural events before the equilibrium shear angle reached, the chip morphology would be still continuous but with severe shear deformation in the secondary shear zone. However, as the cutting speed increased further, the microstructural events, such as dynamic recrystallization and phase transformation, are found to occur before the equilibrium shear angle reached the steady state condition for constant chip thickness cannot be met. The shear angle would vary between the equilibrium shear angle for the work-hardened workpiece and the equilibrium shear angle for the microstructural-softened workpiece, resulting in discontinuous serrated chip morphology. The onset of microstructural softening event occurs when the temperature corrected strain rate exceeds the critical value for dynamic recrystallization or the temperature exceeds phase transformation. The onset of deviation from continuous chip morphology is related to the onset of microstructural softening event in the secondary shear

zone that intervenes before equilibrium shear angle for steady state is reached in accordance with Oxley's model.

Acknowledgment This work was supported by a grant from the National Nature Science Foundation of China (51175003)

References

1. Nomani J, Pramanik A, Hilditch T, Littlefair G (2015) Chip formation mechanism and machinability of wrought duplex stainless steel alloys. The International Journal of Advanced Manufacturing Technology 1–9
2. Ye GG, Chen Y, Xue SF, Dai LH (2014) Critical cutting speed for onset of serrated chip flow in high speed machining. Int J Mach Tools Manuf 86:18–33
3. Nouari M, Molinari A (2005) Experimental verification of a diffusion tool wear model using a 42CrMo4 steel with an uncoated cemented tungsten carbide at various cutting speeds. Wear 259(7): 1151–1159
4. Oxley PLB (1989) The mechanics of machining: an analytical approach to assessing machinability. Ellis Horwood Ltd., England
5. Karpat Y, Özel T (2006) Predictive analytical and thermal modeling of orthogonal cutting process—part II: effect of tool flank wear on tool forces, stresses, and temperature distributions. J Manuf Sci Eng 128(2):445–453
6. Quiza R, Figueira L, Davim JP (2008) Comparing statistical models and artificial neural networks on predicting the tool wear in hard machining D2 AISI steel. Int J Adv Manuf Technol 37(7–8):641–648
7. Kagnaya T, Boher C, Lambert L, Lazard M, Cutard T (2014) Microstructural analysis of wear micromechanisms of WC–6Co cutting tools during high speed dry machining. Int J Refract Met Hard Mater 42:151–162
8. Rowe GW, Spick PT (1967) A new approach to determination of the shear-plane angle in machining. J Manuf Sci Eng 89(3):530–538
9. Oxley PLB, Hastings WF (1977) Predicting the strain rate in the zone of intense shear in which the chip is formed in machining from the dynamic flow stress properties of the work material and the cutting conditions. Proc R Soc Lond A Math Phys Sci 356(1686): 395–410
10. Subramanian SV, Gekonde HO, Zhu G, Zhang X (2002) Role of microstructural softening events in metal cutting. Mach Sci Technol 6(3):353–364
11. Subramanian SV, Gekonde HO, Zhu G, Zhang X, Urlau U, Roelofs H (2004) Inclusion engineering of steel to prevent chemical tool wear. Ironmak Steelmak 31(3):249–257
12. Adibi-Sedeh AH, Madhavan V, Bahr B (2003) Extension of Oxley's analysis of machining to use different material models. J Manuf Sci Eng 125(4):656–666
13. Calamaz M, Coupard D, Nouari M, Girot F (2011) Numerical analysis of chip formation and shear localisation processes in machining the Ti-6Al-4V titanium alloy. Int J Adv Manuf Technol 52(9–12): 887–895
14. Jaspers SPFC, Dautzenberg JH (2002) Material behaviour in conditions similar to metal cutting: flow stress in the primary shear zone. Int J Mater Prod Technol 122(2):322–330
15. Gekonde HO, Subramanian SV (2002) Tribology of tool–chip interface and tool wear mechanisms. Surf Coat Technol 149(2):151–160
16. Jonas JJ, Quelennec X, Jiang L, Martin É (2009) The avrami kinetics of dynamic recrystallization. Acta Mater 57(9):2748–2756
17. Pu CL, Zhu GH, Tao, YL, Yang SB (2015) Modeling of hot deformation behavior with dynamic recrystallization in TC4 titanium alloy. Int J Mater Res, pp 1–7
18. Ma Q, Lin ZQ, Yu ZQ (2009) Prediction of deformation behavior and microstructure evolution in heavy forging by FEM. Int J Adv Manuf Technol 40(3–4):253–260
19. Courbon C, Mabrouki T, Rech J, Mazuyer D, Perrard F, D'Eramo E (2013) Towards a physical FE modelling of a Dry cutting operation: influence of dynamic recrystallization when machining AISI 1045. Procedia CIRP 8:516–521